Preparation and optical properties of poly(vinylidene difluoride)/$(Y_{0.97}Eu_{0.03})_2O_3$ rare-earth nanocomposite

Chunhua Xu (许春华), Runping Jia (贾润萍), Chunfa Ouyang (欧阳春发), Xia Wang (王 霞), and Guoying Yao (姚国英)

Department of Materials Science and Engineering, Shanghai Institute of Technology, Shanghai 200235

Received July 16, 2008

In this letter, poly(vinylidene difluoride) (PVDF)/$(Y_{0.97}Eu_{0.03})_2O_3$ rare-earth nanocomposites were prepared by a simple co-precipitation method, and their morphology, structure, and optical properties were investigated. The scanning electron microscope (SEM) images showed that the $(Y_{0.97}Eu_{0.03})_2O_3$ rare-earth nanoparticles formed 50 nm — 2 μm aggregates in PVDF matrices. X-ray diffraction (XRD) curves indicated the incorporation and structure preserving of $(Y_{0.97}Eu_{0.03})_2O_3$ nanoparticles in PVDF matrices. Photoluminescence (PL) spectra of the nanocomposite showed a characteristic red light emission at 612 nm, which was attributed to the intrinsic emission of $(Y_{0.97}Eu_{0.03})_2O_3$ nanoparticles. Optical band gap (E_g) of the nanocomposite exhibited a decreasing trend with the increase of $(Y_{0.97}Eu_{0.03})_2O_3$ content in PVDF matrices within the experimental dosage range.

OCIS codes: 160.5690, 160.2540, 250.5230.
doi: 10.3788/COL20080610.0763.

As excellent rare-earth luminescent materials, europium (Eu) (III) complexes and oxides particles have been attracting attention since Samelson and Lempicki reported the first successful laser action in 1963[1−3]. In recent years, some works were focused on the polymer based composite containing Eu (III) complexes due to their excellent luminescent properties and potential applications in fluorescent probes, waveguides, optical fiber amplifiers, and organic light-emitting diodes (OLEDs)[4−7]. Till now, various techniques have been developed for synthesizing composites containing Eu_2O_3. For example, by using supercritical CO_2/ethanol solution, Wang *et al.* prepared polymer/Eu_2O_3 composites via decomposition of europium nitrate hexahydrate[8], Fu *et al.* obtained crystalline Eu_2O_3 nanotubes coated on carbon nanotubes and studied its photoluminescence (PL) spectrum[9], and Cannas *et al.* synthesized $(Eu_2O_3)Y_2O_3$-SiO_2 nanocomposites by sol-gel method and studied their luminescence spectra[10,11]. In this letter, poly(vinylidene difluoride) (PVDF)/$(Y_{0.97}Eu_{0.03})_2O_3$ (the molar ratio of yttrium (Y) to Eu is 97:3) nanocomposites were prepared by a simple co-precipitation method with the aid of ultrasonic technique. The morphology, structure, and optical properties of the nanocomposites were studied. PVDF is a multipurpose polymer used in piezoelectric and pyroelectric materials[12], nonlinear optics[13], ultrafiltration membrane[14], and dye-sensitized solar cells as a solid polymer electrolyte[15], therefore, it can be very interesting to combine the unique properties of PVDF and $(Y_{0.97}Eu_{0.03})_2O_3$ rare-earth nanoparticle to prepare the nanocomposite. So far as we know, no detailed investigation on the preparation of such a luminescent nanocomposite by co-precipitation method has been reported in the literature. PVDF/$(Y_{0.97}Eu_{0.03})_2O_3$ nanocomposite with unique optical properties would promote the applications of rare-earth materials.

The preparation processes were briefly described as follows: firstly, the definite amount of PVDF was dissolved in N,N-dimethyl acetamide (DMAc) by magnetic stirring and sonication, and the $(Y_{0.97}Eu_{0.03})_2O_3$ nanoparticles were dispersed in DMAc; next, the PVDF-DMAc solution and $(Y_{0.97}Eu_{0.03})_2O_3$-DMAc dispersions were mixed and sonicated together; then the mixtures were poured into the deioned water as nonsolvent to co-precipitate PVDF/$(Y_{0.97}Eu_{0.03})_2O_3$ nanocomposite; after filtration, the recovered nanocomposites were washed using water and anhydrous ethanol in sequence, vacuum-desiccated, and hot-pressed to get thin slices for characterization.

Sizes and structures of the $(Y_{0.97}Eu_{0.03})_2O_3$ nanoparticles were characterized by transmission electron microscope (TEM) using JEOL-200CX (Japan) operated at 200 kV. Fracture sections and dispersion state of the $(Y_{0.97}Eu_{0.03})_2O_3$ nanoparticles in PVDF matrices were observed by scanning electron microscope (SEM) using Hitachi S-4500 (Japan). The fracture samples were prepared by cooling and breaking the slices in liquid nitrogen, and were coated with carbon for SEM analysis. X-ray diffraction (XRD) of the samples was performed with a Bruker D8-Advance diffractometer (Germany) using Cu K_α radiation, to assess structural changes of the nanocomposite. The excitation and emission spectra were conducted on Cary Eclipse fluorescence spectrophotometer (USA), and the ultraviolet visible spectra (UV-Vis) were recorded with a Shimadzu UV-2100 instrument (Japan).

Figure 1(a) shows the TEM image of the $(Y_{0.97}Eu_{0.03})_2O_3$ nanoparticles. It can be seen that the sizes of the nanoparticles concentrate on about 20 − 40 nm. Figures 1(b)—(d) show the SEM images of the fracture surfaces of pure PVDF and PVDF/$(Y_{0.97}Eu_{0.03})_2O_3$ nanocomposite slices with 1 and 5 wt.-% $(Y_{0.97}Eu_{0.03})_2O_3$ nanoparticles, respectively. A contrast analysis of the SEM images of pure PVDF and nanocomposite indicates that $(Y_{0.97}Eu_{0.03})_2O_3$ particles are dispersed into the PVDF matrices shown as white parts in gray PVDF matrices. From the scale bar,

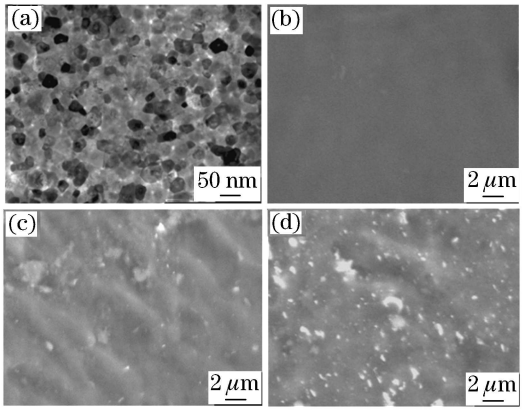

Fig. 1. (a) TEM image of the $(Y_{0.97}Eu_{0.03})_2O_3$ nanoparticles; SEM images of the fracture sections of (b) pure PVDF, PVDF/$(Y_{0.97}Eu_{0.03})_2O_3$ nanocomposite slices with (c) 1 wt.-% and (d) 5 wt.-% $(Y_{0.97}Eu_{0.03})_2O_3$ nanoparticles.

it can be seen that the sizes of $(Y_{0.97}Eu_{0.03})_2O_3$ particles dispersed in the PVDF matrices are $50-500$ nm at the 1 wt.-% $(Y_{0.97}Eu_{0.03})_2O_3$ content and 150 nm — 2 μm at the 5 wt.-% content. With the increase of the content, the $(Y_{0.97}Eu_{0.03})_2O_3$ particles in PVDF matrices obviously turn big. Compared with the sizes of the pristine $(Y_{0.97}Eu_{0.03})_2O_3$ nanoparticles, it can be concluded that these particles are some aggregates of the pristine ones. However, when the $(Y_{0.97}Eu_{0.03})_2O_3$ content is lower than 1 wt.-%, the $(Y_{0.97}Eu_{0.03})_2O_3$ particles cannot be observed under the SEM, which suggests that the $(Y_{0.97}Eu_{0.03})_2O_3$ nanoparticles are better dispersed in PVDF matrices. In a word, the state of dispersion and size distribution of the $(Y_{0.97}Eu_{0.03})_2O_3$ aggregates in PVDF matrices are greatly relevant with the $(Y_{0.97}Eu_{0.03})_2O_3$ content.

Figure 2 shows the XRD patterns of $(Y_{0.97}Eu_{0.03})_2O_3$ nanoparticle powder, pure PVDF, and nanocomposite with different $(Y_{0.97}Eu_{0.03})_2O_3$ contents. It can be seen that the diffraction peaks at 33.3°, 48.1°, and 57.1° become more and more prominent when the $(Y_{0.97}Eu_{0.03})_2O_3$ content increases, which is attributed to the characteristic diffraction of the $(Y_{0.97}Eu_{0.03})_2O_3$ particles. Moreover, the peak at 28.9° turns intenser and broader with the increase of the $(Y_{0.97}Eu_{0.03})_2O_3$ content, which is derived from the combined diffraction of PVDF and the particles. These results indicate the incorporation of $(Y_{0.97}Eu_{0.03})_2O_3$ nanoparticles in PVDF matrices. In addition, there is no new peak found in the diffraction curves except for those of PVDF and $(Y_{0.97}Eu_{0.03})_2O_3$, which shows that there is no new phase forming.

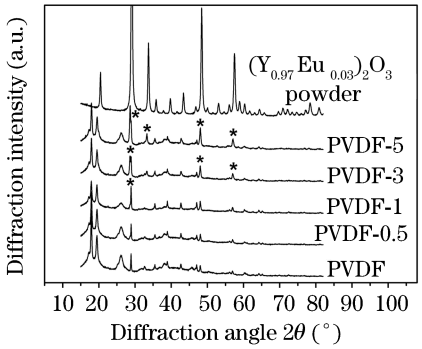

Fig. 2. XRD patterns of $(Y_{0.97}Eu_{0.03})_2O_3$ powder, pure PVDF, and PVDF/$(Y_{0.97}Eu_{0.03})_2O_3$ nanocomposite with different $(Y_{0.97}Eu_{0.03})_2O_3$ contents of 0.5 wt.-% (PVDF-0.5), 1 wt.-% (PVDF-1), 3 wt.-% (PVDF-3), and 5 wt.-% (PVDF-5), respectively.

Figure 3 shows excitation spectrum and emission spectra of the PVDF/$(Y_{0.97}Eu_{0.03})_2O_3$ nanocomposite. In order to choose the excitation wavelength during the emitting tests, excitation spectrum of the nanocomposite sample with 3 wt.-% $(Y_{0.97}Eu_{0.03})_2O_3$ was firstly measured shown in Fig. 3(a), and the emission wavelength was fixed at 612 nm. The excitation spectrum shows that the intensest emission peak emerges at 230 nm, so the wavelength is chosen as excitation wavelength in the emission spectra shown in Fig. 3(b). The emission spectra show a clear red light emission peak at 612 nm attributed to intrinsic luminescence of the $(Y_{0.97}Eu_{0.03})_2O_3$ nanoparticles dispersed in PVDF matrices. With the increase of $(Y_{0.97}Eu_{0.03})_2O_3$ content, other characteristic emission peaks also become distincter and intenser at 533, 552, 588, and 630 nm. These results suggest that PL property of the nanocomposites is endowed by $(Y_{0.97}Eu_{0.03})_2O_3$ rare-earth nanoparticles, and the PVDF acts as support. The PL spectra can be described to the well known $^5D_0 \rightarrow {}^7F_J$ line emission ($J = 0, 1, 2, \cdots$) of the Eu^{3+} ion with the strongest emission at $610-612$ nm[2,6,16], and the red emission (612 nm) can be assigned to the $^5D_0 \rightarrow {}^7F_2$ forced electric dipole transition[16] and radiative transition[17].

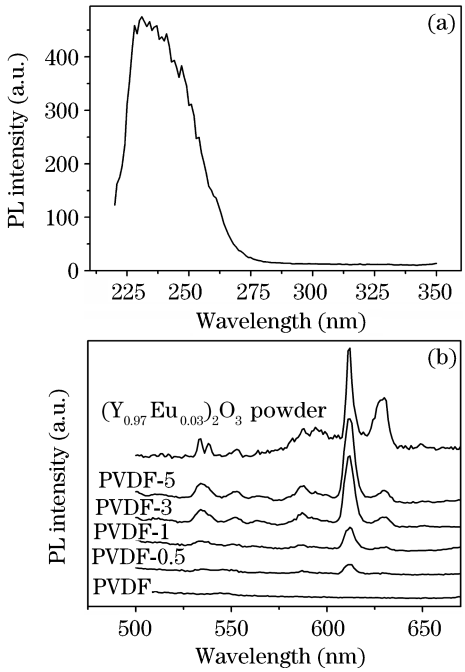

Fig. 3. (a) Excitation spectrum of the PVDF/$(Y_{0.97}Eu_{0.03})_2O_3$ nanocomposite with 3 wt.-% $(Y_{0.97}Eu_{0.03})_2O_3$ nanoparticles, and the emission wavelength was fixed at 612 nm; (b) emission spectra of the PVDF/$(Y_{0.97}Eu_{0.03})_2O_3$ nanocomposite with different $(Y_{0.97}Eu_{0.03})_2O_3$ contents of 0.5 wt.-% (PVDF-0.5), 1 wt.-% (PVDF-1), 3 wt.-% (PVDF-3), and 5 wt.-% (PVDF-5), respectively, and the excitation wavelength was fixed at 230 nm.

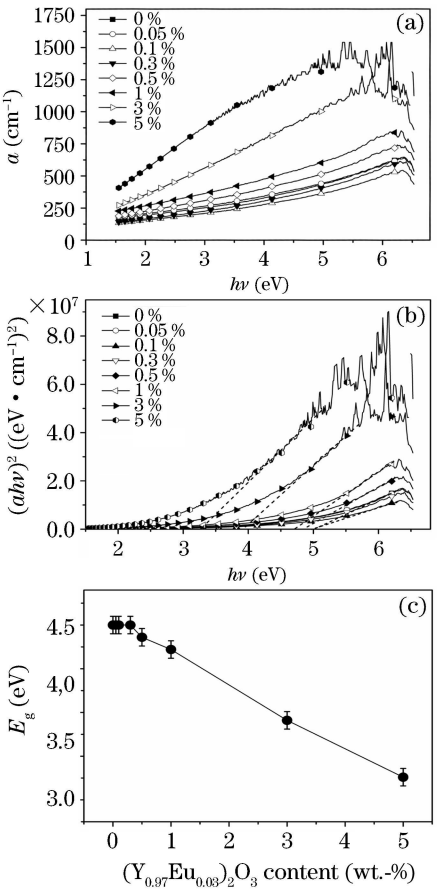

Fig. 4. (a) Variation of α and (b) variation of $(\alpha h\nu)^2$ of the PVDF/$(Y_{0.97}Eu_{0.03})_2O_3$ nanocomposite with $h\nu$ at different $(Y_{0.97}Eu_{0.03})_2O_3$ contents; (c) E_g of the PVDF/$(Y_{0.97}Eu_{0.03})_2O_3$ nanocomposite with the $(Y_{0.97}Eu_{0.03})_2O_3$ content.

The optical band gap (E_g) of the nanocomposite was investigated based on the data processing and analysis of the UV-Vis spectra. According to Refs. [18 – 20], optical absorption coefficient (α) can be obtained from the transmittance date shown in Fig. 4(a), and E_g can be obtained by extrapolating from the curve variation of $(\alpha h\nu)^2$ with the photon energy ($h\nu$) shown in Fig. 4(b). Figure 4(a) indicates an increasing trend of α with the increase of $h\nu$ and $(Y_{0.97}Eu_{0.03})_2O_3$ content. When the $(Y_{0.97}Eu_{0.03})_2O_3$ content is lower than 0.5 wt.-%, the α variation is not regular, which is probably related to the preparation processes. Figure 4(c) shows the variation of E_g with the increase of $(Y_{0.97}Eu_{0.03})_2O_3$ content. The error bars were brought in the processes of extrapolating. It shows that the E_g only fluctuates within the range of 0.14 eV when the $(Y_{0.97}Eu_{0.03})_2O_3$ content is less than 0.5 wt.-%. While the $(Y_{0.97}Eu_{0.03})_2O_3$ content increases to 5 wt.-%, the E_g decreases by 1.74 eV compared with that of pure PVDF. This indicates that the E_g tend to decrease with the increase of $(Y_{0.97}Eu_{0.03})_2O_3$ content within the experimental dosage range. Similar behavior was observed on the optical study of PVDF/$MgCl_2$ system by Tawansi *et al.*[21] and polyvinylchlo-ride/polyethylene oxide (PVC/PEO) system by Al-Ramadin[22]. The two systems contained electrolyte filler $MgCl_2$ and electrolyte PEO polymer, and they thought that the decrease of optical energy gap was caused by the ionic contribution of electrolyte content in the electrical process. Our PVDF/$(Y_{0.97}Eu_{0.03})_2O_3$ system do not contain electrolyte component, and the mechanism cannot be clarified at present and the related study is ongoing now.

In conclusion, we have prepared PVDF/$(Y_{0.97}Eu_{0.03})_2O_3$ rare-earth nanocomposites by a simple co-precipitation method with the aid of ultrasonic technique. The morphology analysis showed that the $(Y_{0.97}Eu_{0.03})_2O_3$ nanoparticles were dispersed as 50 nm — 2 μm aggregates in PVDF matrices, and the structure analysis indicated that $(Y_{0.97}Eu_{0.03})_2O_3$ nanoparticles were incorporated in PVDF matrices with preserved structure. A red light emission feature at 612 nm ascribed to the intrinsic luminescence of $(Y_{0.97}Eu_{0.03})_2O_3$ nanoparticles was clearly observed in the emission spectra of the nanocomposite. The optical band gap tended to decrease with the increase of $(Y_{0.97}Eu_{0.03})_2O_3$ content within the experimental dosage range. Further investigation on the nature and mechanism of the optical properties is ongoing and to be reported in the following articles.

This work was supported by the Key Subject Construction Project in Shanghai (No. p1502) and the Foundation of the Shanghai Institute of Technology (No. YJ2007-37). The authors are very grateful to Professor Zhengjun Zhang and Professor Zhengcao Li for their help and discussion, and grateful to Professor Yunhan Ling, Professor Ming Li, and Professor Cewen Nan for their help in preparation processes. C. Xu's e-mail address is chhxu@sit.edu.cn.

References

1. H. Samelson and A. Lempicki, J. Chem. Phys. **39,** 110 (1963).
2. A. Pandey, A. Pandey, M. K. Roy, and H. C. Verma, Mater. Chem. Phys. **96,** 466 (2006).
3. G. Yao, L. Su, X. Xu, L. Zheng, and J. Xu, Chin. Opt. Lett. **6,** 133 (2008).
4. R. Pogreb, O. Popov, V. Lirtsman, O. Pyshkin, A. Kazachkov, A. Musin, G. Whyman, B. Finkelshtein, Y. Shmukler, D. Davidov, A. Gladkikh, and E. Bormashenko, Polym. Adv. Technol. **17,** 20 (2006).
5. H. Liang, B. Chen, F. Q. Guo, J. B. Guan, Q. J. Zhang, and Z. Z. Li, Phys. Stat. Sol. (b) **242,** 1087 (2005).
6. H. G. Liu, Y. I. Lee, W. P. Qin, K. Jang, S. Kim, and X. S. Feng, J. Appl. Polym. Sci. **92,** 3524 (2004).
7. G. Ramachandran, G. Simon, Y. B. Cheng, T. A. Smith, and L. M. Dai, J. Fluoresc. **13,** 427 (2003).
8. J. Q. Wang, C. L. Zhang, Z. M. Liu, K. L. Ding, and Z. Z. Yang, Macromol. Rapid Commun. **27,** 787 (2006).
9. L. Fu, Z. M. Liu, Y. Q. Liu, B. X. Han, J. Q. Wang, P. A. Hu, L. C. Cao, and D. B. Zhu, Adv. Mater. **16,** 350 (2004).
10. C. Cannas, M. Casu, M. Mainas, A. Musinu, and G. Piccaluga, Compos. Sci. Technol. **63,** 1175 (2003).
11. C. Cannas, M. Casu, A. Musinu, G. Piccaluga, and A. Speghini, and M. Bettinelli, J. Non-cryst. Solids **306,** 193 (2002).
12. B. R. Hahn and J. H. Wendorff, Polymer **26,** 1611 (1985).
13. L. Priya and J. P. Jog, J. Polym. Sci. Part B **40,** 1682 (2002).

14. Y. Lu, S. L. Yu, and B. X. Chai, Polymer **46,** 7701 (2005).
15. S. Anandan, S. Pitchumani, B. Muthuraaman, and P. Maruthamuthu, Sol. Energ. Mater. Sol. Cells **90,** 1715 (2006).
16. Z. L. Fu, S. H. Zhou, T. Q. Pan, and S. Y. Zhang, J. Lumin. **124,** 213 (2007).
17. M. K. Chong, K. Pita, and C. H. Kam, J. Phys. Chem. Solids **66,** 213 (2005).
18. Z. Yang, L. Luo, and W. Chen, Acta Opt. Sin. (in Chinese) **27,** 598 (2007).
19. T. Toyoda, H. Nakanishi, S. Endo, and T. Irie, J. Phys. D **18,** 747 (1985).
20. T. Toyoda, S. Maruyama, H. Nakanishi, S. Endo, and T. Irie, J. Phys. D **19,** 909 (1986).
21. A. Tawansi, A. H. Oraby, E. M. Abdelrazek, and M. Abdelaziz, Polym. Testing **18,** 569 (1999).
22. Y. Al-Ramadin, Opt. Mater. **14,** 287 (2000).